

# Dynamics in the satellite system of Triangulum: Is AndXXII a dwarf satellite of M33?

S. C. Chapman,<sup>1</sup> L. Widrow,<sup>2</sup> M. L. M. Collins,<sup>3,1</sup> J. Dubinski,<sup>4</sup> R. A. Ibata,<sup>5</sup>  
J. Peñarrubia,<sup>6,1</sup> M. Rich,<sup>7</sup> A. M. N. Ferguson,<sup>8</sup> M. J. Irwin,<sup>1</sup> G. F. Lewis,<sup>9</sup> N. Martin,<sup>5,3</sup>  
A. McConnachie,<sup>10</sup> N. Tanvir<sup>11</sup>.

<sup>1</sup> *Institute of Astronomy, Madingley Road, Cambridge, CB3 0HA, U.K.*

<sup>2</sup> *Department of Physics, Engineering Physics and Astronomy, Queen's University, Kingston, Ontario B3H 3C3, Canada*

<sup>3</sup> *Max-Planck-Institut für Astronomie, Königstuhl 17, D-69117 Heidelberg, Germany*

<sup>4</sup> *Department of Astronomy & Astrophysics, University of Toronto, 50 St George Street, Toronto, Ontario, Canada M5S 3H4*

<sup>5</sup> *Observatoire de Strasbourg, 11, rue de l'Université, F-67000, Strasbourg, France*

<sup>6</sup> *Ramón y Cajal Fellow, Instituto de Astrofísica de Andalucía-CSIC, Glorieta de la Astronomía, 18008, Granada, Spain*

<sup>7</sup> *Department of Physics and Astronomy, University of California, Los Angeles, CA 90095-1547*

<sup>8</sup> *Institute for Astronomy, University of Edinburgh, Royal Observatory, Blackford Hill, Edinburgh, UK EH9 3HJ*

<sup>9</sup> *Sydney Institute for Astronomy, School of Physics, A29, University of Sydney, NSW 2006, Australia*

<sup>10</sup> *NRC Herzberg Institute of Astrophysics, 5071 West Saanich Road, Victoria, British Columbia, Canada V9E 2E7*

<sup>11</sup> *Department of Physics & Astronomy, University of Leicester, Leicester, LE17RH, UK*

27 September 2012

## ABSTRACT

We present results from a spectroscopic survey of the dwarf spheroidal And XXII and the two extended clusters EC1 and EC2. These three objects are candidate satellites of the Triangulum galaxy, M33, which itself is likely a satellite of M31. We use the DEep Imaging Multi-Object Spectrograph mounted on the Keck-II telescope to derive radial velocities for candidate member stars of these objects and thereby identify the stars that are most likely actual members. Eleven most probable stellar members (of 13 candidates) are found for And XXII. We obtain an upper limit of  $\sigma_v < 6.0 \text{ km s}^{-1}$  for the velocity dispersion of And XXII,  $[\text{Fe}/\text{H}] \sim -1.6$  for its metallicity, and 255 pc for the Plummer radius of its projected density profile. We construct a colour magnitude diagram for And XXII and identify both the red giant branch and the horizontal branch. The position of the latter is used to derive a heliocentric distance to And XXII of  $853 \pm 26 \text{ kpc}$ . The combination of the radial velocity, distance, and angular position of And XXII indicates that it is a strong candidate for being the first known satellite of M33 and one of the very few examples of a galactic satellite of a satellite. N-body simulations imply that this conclusion is unchanged even if M31 and M33 had a strong encounter in the past few Gyr. We test the hypothesis that the extended clusters highlight tidally stripped galaxies by searching for an excess cloud of halo-like stars in their vicinity. We find such a cloud for the case of EC1 but not EC2. The three objects imply a dynamical mass for M33 that is consistent with previous estimates.

**Key words:** M 33 – M 31 – Dwarf Galaxies – DEIMOS

## 1 INTRODUCTION

Dwarf spheroidal galaxies (dSphs) probe the outer regions of their host galaxies, and as such act as important tracers of the dark matter halo at large galacto-centric radii (e.g., Evans & Wilkinson 2000, Watkins, Evans & An 2010). Further, dSphs are the progenitors of tidal streams found within the halos of the Milky Way (e.g., Belokurov et al. 2006, 2007) and Andromeda (e.g., Ibata et al. 2001, 2004,

2007; Chapman et al. 2006, 2008; McConnachie et al. 2009), which help to trace their orbits. Modelling tidal disruption of dwarfs provides another way to constrain the dark halos of their host galaxies. DSphs can also be used as a test of our understanding of hierarchical clustering processes, including the evolution of these systems, and their survival in the environments of much larger dark matter haloes (e.g. Sales et al. 2007a,b). Finally, the faint dSph population are believed to be dominated by dark matter, and can therefore provide

useful laboratories to study the properties of dark matter itself (e.g., Peñarrubia et al. 2007,2008).

And XXII, a faint dSph galaxy that lies in the Triangulum constellation, was discovered by Martin et al. (2009) using the Pan-Andromeda Archeological Survey (PAndAS – McConnachie et al. 2009). The proximity of And XXII (42 kpc in projection) to the Triangulum galaxy (M33), in conjunction with its large distance from M31 (224 kpc, also in projection), led Martin et al. (2009) to speculate that this dwarf galaxy could in fact be the first discovered satellite dSph of M33. However, at that point, no spectroscopic data were available for the dwarf, and neither the radial velocity nor a robust line of sight distance were known.

M33 may well have had a close passage by M31 and therefore And XXII could have been influenced by two more massive galaxies. The existence of a satellite at this radius would place a constraint on the strength of an M33–M31 interaction (McConnachie et al., 2009, Dubinski et al., in prep) since such an interaction naturally strips material from the outer parts of M33. If And XXII were shown to be a satellite of M33, then this would make M33 one of the smallest galaxies known to have a satellite, and it would make M31–M33–And XXII one of the first examples of a three-level galaxy hierarchy, a phenomenon that naturally arises in the hierarchical clustering scenario of structure formation, and a topic of considerable interest for predictions of cold dark matter (CDM) models (Sales et al. 2007a; d’Onghia et al. 2010). And XXII would also expand the known halo size of the M33 system by 50%, from its recently discovered outermost globular cluster (Huxor et al. 2009), and consistent with an extended stellar halo profile to large radius (Cockcroft et al. 2012).

Assessing the number of expected bound satellites to a host galaxy of a given mass is not a straightforward exercise, as even moderate mass galaxies are heavily influenced by any larger galaxies they may have interacted with (e.g., Purcell et al. 2009). M33 is a modest spiral galaxy with a mass ( $M_{\text{dyn}} \sim 10^{11} M_{\odot}$ ) approximately one tenth the mass of M31. It resides at a projected distance of 204 kpc from the centre of M31, presumably well-inside the M31 dark halo and measurements of its line-of-sight velocity and proper motion suggest that it is on a highly elongated orbit around M31. The implication is that M33 is a satellite of M31 and likely passed much closer to M31 in the past than its present distance (but see Loeb et al. 2005). This association is supported by the existence of a strong warp and heavily disturbed HI disk in M33 (Rogstad et al. 1976; Putman et al. 2009), as well as the presence of a stellar stream extending from its stellar disk (McConnachie et al. 2009, 2010). Interactions are likely important with galaxies like M33, influencing the number of bound dSphs.

Through complete observations of a sample of nearby spiral galaxies, Erickson, Gottesman, & Hunter (1999) typically find at least one massive satellite comparable to the LMC of spiral galaxies down to  $V_{r,\text{max}}=140 \text{ km s}^{-1}$ . But the lowest mass galaxies in this survey are still more than twice as massive than M33, which has  $V_{r,\text{max}} \sim 100 \text{ km s}^{-1}$  from the stellar rotation curve out to 13 kpc (Trethewey 2011). Guo et al. (2011) also attempt to characterize the satellite fractions in N-body simulations as a function of stellar mass, finding moderate mass galaxies like M33 found close to larger galaxies (like M31) are often deficient in bound

satellites. Extrapolating the Guo et al. (2011) results, M33 (with a stellar mass of  $3\text{--}6 \times 10^9 M_{\odot}$ ) might be expected to have as many as 20 dSph satellites based on  $\Lambda$ CDM (Cold Dark Matter) predictions, but in fact has only one candidate dSph out to a radius of 50 kpc projected, And XXII, and this remains to be confirmed. The lack of satellite dwarfs discovered around M33 may suggest that it has been orbiting M31 for long enough to have had its satellites stripped by the more massive galaxy, and now indistinguishable from M31’s satellites.

While And XXII is the only candidate dSph satellite of M33, there are other distant star clusters in the halo of M33 which may signpost, or even be the remnants of disrupted satellites. The two ‘extended clusters’, M33-EC1 (Stonkute et al. 2008 – hereafter EC1) and HM33-A (Huxor et al. 2009 – hereafter EC2), lying in projection at 13 kpc and 28 kpc respectively in M33’s halo, represent just such a possibility. These intriguing objects have no analogs in the Milky Way (MW) sub-system. One extended cluster in the M31 halo, EC4, has been studied spectroscopically (Collins et al. 2009). EC4 lies within the ‘stream Cp’ tidal stream in M31’s halo, and the kinematics and metallicity of EC4 bear a striking resemblance to ‘stream Cp’ (Ibata et al. 2007; Chapman et al. 2008) which has the same radial velocity and metallicity, suggesting that the two are very likely related. However, there was no evidence that EC4 contained a substantial dark matter component to suggest it was the remnant of a dSph galaxy, and EC4 was classified as a stellar cluster with a large (30 pc) core radius. The extended clusters (and outer halo clusters in general) have been found to preferentially lie in regions of excess stars suggestive of tidal debris in the halo of M31 (Mackey et al. 2010), and the large size of ECs may be a byproduct of the disruption of their host galaxies. In the context of M33’s dynamical mass, satellite system and accretion history, it is thus of interest to study its EC1 and EC2, and search for possible evidence of disrupted hosts in their vicinity.

Whether And XXII, as well as EC1 and EC2, are likely to orbit M33 depends on their kinematics and real distance from the two possible hosts. These issues can be addressed via the radial velocities of the brightest Red Giant Branch (RGB) stars, which in turn confirm whether the brightest stars are likely to be members. Tollerud et al. (2012) presented radial velocities of 7 stars in And XXII as part of their survey of M31 dSphs, noting that it might be a candidate for a satellite of M33. The distance to And XXII can also be corroborated and more precisely constrained by photometry reaching the stellar horizontal branch. In conjunction with simulations investigating the bound particles and the gravitational forces of M31 and M33 on And XXII, we can attempt to determine whether And XXII is an M33 satellite.

To address the question of And XXII’s parent galaxy and the detailed properties of the dSph itself, we have analyzed the optical imaging from PAndAS (McConnachie et al. 2009), and used the DEep Imaging Multi-Object Spectrograph (DEIMOS) on Keck II to derive radial velocities and metallicities of stars within And XXII. To complete the picture of satellites of M33, we have also obtained spectroscopic observations of EC1 and EC2 (two likely additions to the M33 satellite system), in order to establish their radial velocities and constrain the halo mass of M33, as well as search for the signatures of dark matter or tidal streams

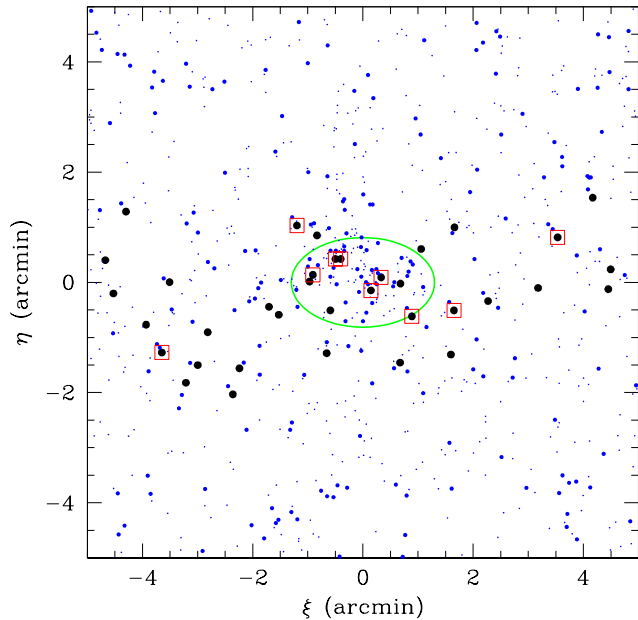


**Figure 1.** Spatial distribution of stars in the region of And XXII. All stars in the PAndAS survey (small blue dots) contrast the centrally concentrated subset with colours and magnitudes consistent with metal-poor red giant branch populations at the distance of M31 (larger blue dots). All stars lying in the DEIMOS mask are shown (large black filled circles), while candidate member stars identified spectroscopically are highlighted (red squares). Member stars were identified probabilistically as described in text and Collins et al. (2012). The central ellipse corresponds to the region within two half-light radii of the dwarf galaxy using structural parameters listed in Table 1.

associated with them. In this work, we assume heliocentric distances to M31 and M33 respectively of  $779 \pm 19$  kpc and  $820 \pm 19$  kpc, (Conn et al. 2012), consistent with distances to M33 previously estimated (e.g., McConnachie et al. 2004, Tiede et al., 2004).

## 2 OBSERVATIONS

Multi-object Keck observations with DEIMOS (Faber et al. 2001) for And XXII were made on 2009 Sept. 23 and 2010 Sept. 9. The first set of observations had  $0.8''$  seeing and total mask exposure times of 20min while the second set had  $0.6''$  seeing and 60min exposure times. The extended clusters, EC1 and EC2, were also observed on 2009 Sept. 23 for 45min each. We use the 1200 line/mm grating where the spectral resolution in the red is  $R \sim 6000$  and the observed wavelength range is  $0.65 - 0.93 \mu\text{m}$ . Data reduction for the spectra followed standard techniques using the DEIMOS-DEEP2 pipeline (Faber et al. 2003) and included debiasing, flat-fielding, extracting, wavelength-calibration and sky-subtraction. The data were also reduced using our custom pipeline (e.g., Ibata et al. 2005) as a check on the extractions and calibrations.

Radial velocities of our target stars were determined by fitting the peak of the cross-correlation function between the observed spectra and a template spectrum. The latter con-

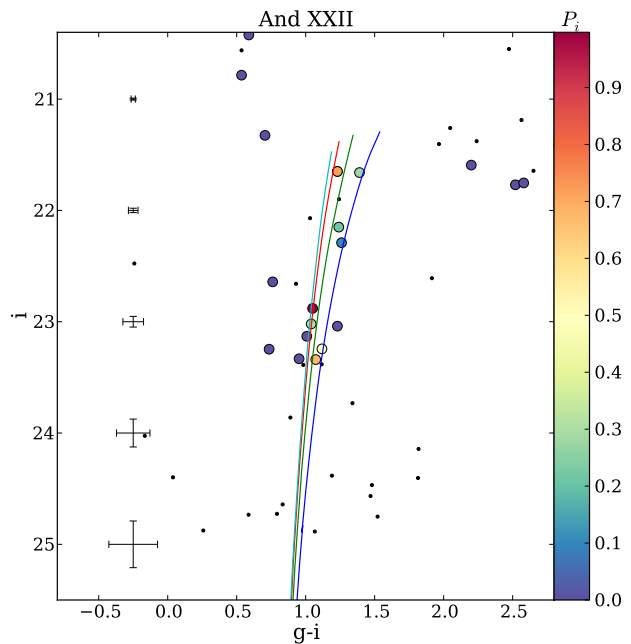


**Figure 2.** CFHT-MegaCam colour-magnitude diagrams of stars showing the DEIMOS targeted stars (large symbols) and all star-like sources within  $2'$  radius (small symbols) centered around And XXII. Dartmouth isochrones, from  $[\text{Fe}/\text{H}] = -1.8$  to  $-1.4$  are overlaid at our derived distance to And XXII. The RGB is clearly visible, while the horizontal branch is just visible although without any likely spectroscopic members (the horizontal branch is however well detected in the  $g$ -band – Fig. 3). Candidate dSph member stars from the DEIMOS spectroscopy are further highlighted (large circles, colour-coded by their probability). Probability of membership to And XXII is defined by a combination of velocity, distance from the RGB locus, and radial distance from the centre of And XXII (see Table 2). The NaI doublet equivalent width was used as an additional discriminant of MW foreground stars, however this did not result in the rejection of any stars not already flagged from the CMD position.

sisted of delta functions smoothed to the instrumental resolution ( $1.3 \text{ \AA}$ ) at the wavelengths of the CaII triplet (CaT) absorption lines. This procedure also provided an estimate of the radial velocity accuracy obtained for each measurement. The velocity uncertainties range from  $4$  to  $17 \text{ km s}^{-1}$ .

Target stars were assigned from a broad (1 mag) box around the general outline of the RGB of the dwarf. A higher priority was given to stars within a narrower box of 0.3 mag around the RGB. In addition, brighter stars were prioritized over fainter ones. The remainder of the mask space was filled with target stars from a broad region that encompassed RGB stars in M31 over all possible metallicities and distances. The And XXII masks had 93 and 173 target stars respectively, while EC1 had 168, and EC2 had 88 target stars.

We followed the procedures outlined in Collins et al. (2010) in order to correct for various systematic errors that arise in the velocity calculations. A template telluric spectrum was constructed from the data, which was cross-correlated with each of our science spectra to determine the

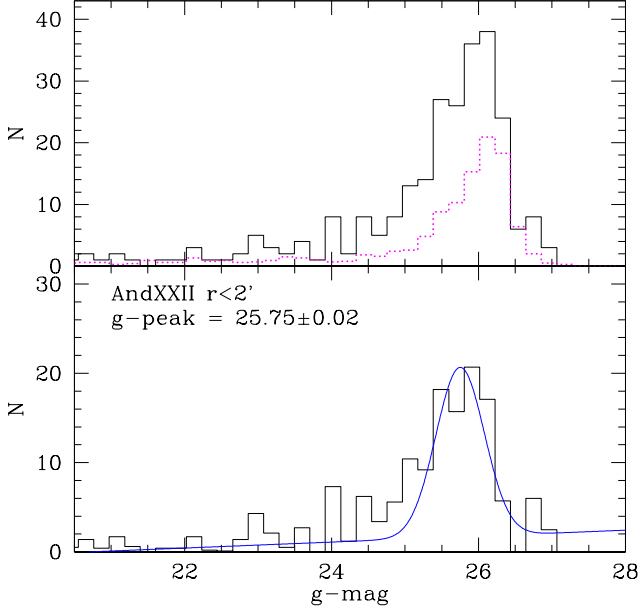


**Figure 3.** Top panel: The  $g$ -band luminosity function of the central regions of AndXXII (black) within two half-light radii, together with suitably scaled (by sky area) much larger neighbouring comparison regions (magenta). No  $g-i$  cut has been applied given the faintness of the HB stars. Bottom panel: Difference luminosity function highlighting the regions around the horizontal branch. The  $g$ -band magnitude of the peak of the fits is consistent at  $g = 25.75 \pm 0.10$  corresponding to a distance of  $853 \pm 26$  kpc, with a measured  $E(B-V)$  of 0.07 extinction in this region. The result is insensitive to a range of radii (from  $r_{1/2}=1-3$  arcmin) used for the luminosity function.

velocity shift caused by systematic errors. For brighter stars ( $i < 21$ ) the velocity corrections are approximately constant. However for fainter stars, where the Signal-to-Noise (S:N) is lower, the magnitude of this telluric correction shows significant scatter about the median value. Evidently, this effect is injecting noise into the velocity measurements. We apply a correction corresponding to a  $2.1 \text{ km s}^{-1}$  offset and a small ( $1.9 \text{ km s}^{-1}$  mask end to end) velocity gradient. This correction is based on measurements of the  $i < 21$  stars in the mask and presumably accounts for a slight mask rotation and positional offset of stars in the slits.

There are twenty-four stars for which the velocity was determined with both of our masks. These repeat observations provide us with a further handle on the velocity measurement errors. In principle, the quantity

$$D_i \equiv \frac{v_{1,i} - v_{2,i}}{(\sigma_{1,i}^2 + \sigma_{2,i}^2)^{1/2}} \quad (1)$$

should be a Gaussian random variable with unit variance. Here, the subscript  $1,i$  refers to the first measurement of the  $i$ 'th star, etc. Likewise,  $\sigma_{1,i}$  is the Monte Carlo error estimate for that measurement. Our procedure is to replace the denominator by  $(\sigma_{1,i}^2 + \sigma_{2,i}^2 + \epsilon^2)^{1/2}$  and adjust the free parameter until the desired distribution is achieved. We find  $\epsilon = 1.6 \text{ km s}^{-1}$ , comparable to that found in other work (e.g.  $2.2 \text{ km s}^{-1}$  in Simon & Geha 2007). We conclude we can

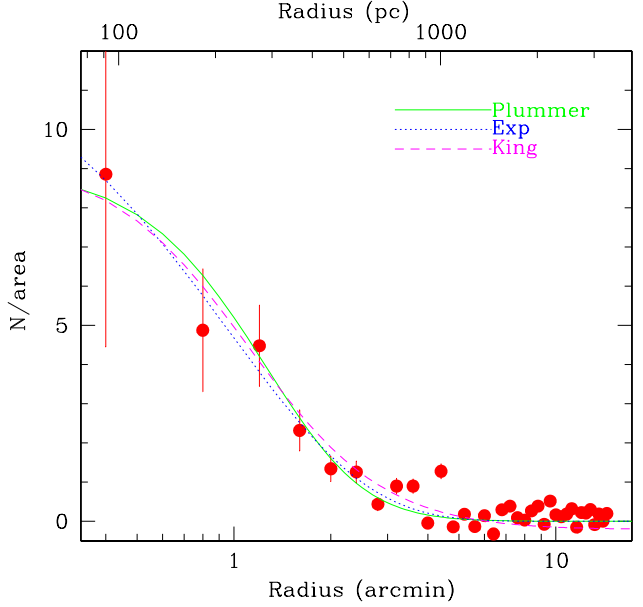


**Figure 4.** Radial profile fits from CFHT-MegaCam extracted stars (with point-like stellar profiles) using  $0.4'$  elliptical annular ring widths for binning, with background subtracted. Using stars with  $20.5 < I < 24.0$  stars we derive  $r_h(\text{Plummer})=1.0 \pm 0.3$  arcmin.

**Table 1.** Derived properties of AndXXII

$\alpha$ (J2000)	$01^{\text{h}}27^{\text{m}}39.9^{\text{s}} \pm 0.6^{\text{s}}$
$\delta$ (J2000)	$28^{\circ}05'28'' \pm 6''$
$D$ (kpc)	$853 \pm 26$
$r_{\text{M31}}$ (kpc)	$258 \pm 31$
$r_{\text{M33}}$ (kpc)	$59^{+21}_{-14}$
$v_r$ ( $\text{km s}^{-1}$ )	$-130.0 \pm 1.7$
$\sigma_v$ ( $\text{km s}^{-1}$ )	$< 6.0, 99.5\% \text{ confidence}$
$\langle [\text{Fe}/\text{H}] \rangle_{\text{phot}}$	$-1.58 \pm 0.04$
$\langle [\text{Fe}/\text{H}] \rangle_{\text{spec}}$	$-1.62 \pm 0.05$
$r_h$ (arcmin)	$1.0 \pm 0.3$
$r_h$ (pc)	$255 \pm 78$
PA (NtoE) ( $^{\circ}$ )	$93 \pm 13$
$\epsilon = 1 - b/a$	$0.55 \pm 0.10$
$L_V$ ( $L_{\odot}$ )	$0.35 \pm 0.05 \times 10^5$
$\mu_{V,0}$ ( $\text{mag/arcsec}^2$ )	$26.7 \pm 0.6$

measure velocities to accuracies of  $\sim 5 \text{ km s}^{-1}$  down to a S:N of 3 or better.

### 3 RESULTS – AND XXII

The spatial distributions of the stars in the region of AndXXII is shown in Figure 1. A central concentration of stars that have colours and magnitudes consistent with a metal-poor RGB population at the distance of M33 is just visible by eye. Spectroscopically targeted stars and candidate member stars (discussed below) are highlighted in Figure 1 and listed in Table 2. In this section, we first analyze the photometry for AndXXII, to assess a distance and mea-

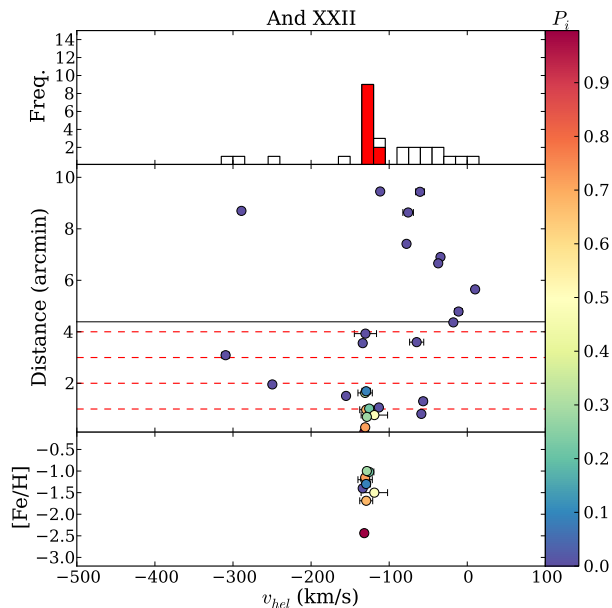


**Figure 5.** Distribution of stars in And XXII as a function of their radial velocity (upper panel). The systemic velocity of M33 ( $-178 \text{ km s}^{-1}$ ) is much closer to And XXII than that of M31 ( $-300 \text{ km s}^{-1}$ ). The stars are then shown as a function of radius from the centre of And XXII, with multiples of the half-light radius drawn as a dashed lines (middle panel). Stars are colour-coded by their membership probability, as in Fig. 2. Photometric  $[\text{Fe}/\text{H}]$  as described in the text is shown on the bottom panels, revealing the tight range in metallicities of And XXII ( $[\text{Fe}/\text{H}] \sim -1.6$ ). Most of the foreground Milky Way stars lie off the grid of isochrones used to calculate  $[\text{Fe}/\text{H}]$ .

sure structural parameters. We then use our spectroscopic survey to constrain candidate member stars and derive the kinematic properties.

### 3.1 Photometry

#### 3.1.1 Distance

The colour-magnitude diagram for And XXII is shown in Figure 2. The And XXII dwarf galaxy is too poorly populated to directly determine its distance using traditional tip of the red giant branch (TRGB) methods, in spite of the fact that our kinematic measurements have secured the brightest RGB stars as dwarf members. Martin et al. (2009) effectively avoided calculating the TRGB distance entirely, while Conn et al. (2012) reveal a ML-TRGB distance with large errors ( $922_{-148}^{+36}$  kpc). To complement the crude TRGB distance, we use the reprocessed CFHT Megacam photometry and exploit the extra depth of the  $g$ -band for bluer stellar populations to directly measure the luminosity of the horizontal branch (HB). This feature accounts for the strong overdensities sloping to fainter magnitudes and bluer colours at the bottom of the Colour-Magnitude Diagram (CMD), e.g. from  $g - i = 1.0, i = 24.8$  to  $g - i = 0.0, i = 25.3$ . The  $i$ -band depth cuts through this region precluding direct isochrone fitting, but we can still exploit the better depth of the  $g$ -band directly by analyzing the  $g$ -band luminosity

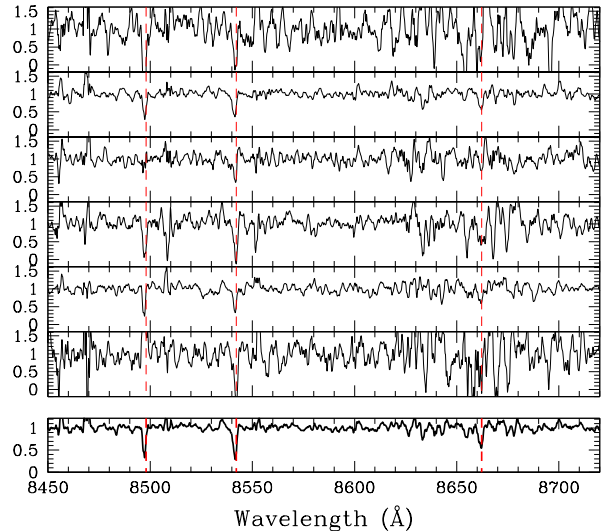


**Figure 6.** Spectra of the six highest probability And XXII member stars, with probability of membership  $>0.3$ , see Collins et al. (2012) for details. The spectra emphasize the well detected CaII triplet lines in each case. The inverse variance weighted summed spectrum is shown in the bottom offset panel.

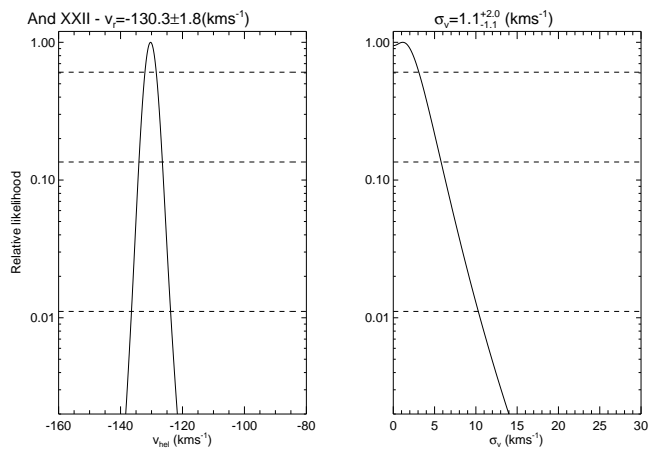


**Figure 7.** Likelihood distributions of member stars in And XXII, showing the dispersion is essentially unresolved with  $v_r = -130.3 \pm 1.8 \text{ km s}^{-1}$ , and  $\sigma_v < 4.0 \text{ km s}^{-1}$ , 95% confidence.

function instead. As a benchmark, the HB magnitude of M31 is  $g_0 = 25.2$ , which for the average extinction in the halo of M31 translates to an apparent magnitude of  $g = 25.4 - 25.5$ . The  $g$ -band data extends down to  $g < 27.0$  mag, where the comparison regions in the CMDs show that there is likely a notable component of contamination from unresolved background galaxies, and careful subtraction of the comparison regions is required to measure the HB mag. The observed  $g$ -band luminosity function (LF) is shown in Fig. 3 along with those of the appropriately scaled (by area) background reference field (from a square degree surrounding And XXII). The bottom panel of Fig. 3 show the  $g$ -band LF with the background subtracted and a best fit Gaussian magnitude.

To calculate the distance modulus we must first estimate a standard absolute magnitude,  $M_g$  for the HB populations typical of dSphs. We adopt a constant of  $M_g = 0.8 \pm 0.1$  in the CFHT MegaCam AB magnitude system, as derived in Richardson et al. (2011). Empirical models which estimate the closely related  $M_v$  of the HB (e.g. Gratton 1998) have been predominantly determined from globular clusters, and have a weak metallicity dependence (gradient) ( $< 0.1$  mag at  $[\text{Fe}/\text{H}] \sim -1.6$ ). The  $g$ -band magnitude of the peak of the fit is  $g = 25.75 \pm 0.10$ , and the extinction corrected distance is  $853 \pm 26$  kpc, with the error calculated by propagating the error in  $M_g$ , the error in the measured location of the HB, and the  $\pm 3\%$  uncertainty in the calibration of the photometry. The luminosities and sizes are updated from Martin et al. (2009) accordingly in Table 1.

### 3.1.2 Structural parameters

Martin et al. (2009) measured a radial profile for And XXII using CFHT Megacam data. Here, we take advantage of improvements in the CFHT image processing to reassess the structural properties of And XXII. We first re-estimate the ellipticity using our magnitude limit  $i < 24$ . Background-corrected radial profiles of And XXII (Figure 4) are then measured using the average stellar density within series of fixed elliptical annuli using the parameters from Table 1. The error bars account for Poisson counting statistics and uncertainties in the derived background level. The overlaid model curves are fits to the data. The best-fit Plummer scale length is  $r_h(\text{plummer}) = 1.0' \pm 0.2'$  when we use stars with  $20.5 < i < 24.0$ . We find that varying the catalog depth from  $i_{\text{max}} = 23$  to  $i_{\text{max}} = 24.5$ , or using the deeper  $g$ -band data has little effect on the fit. The two half-light radius limit is shown in Figure 1. This radius is slightly larger than that found in Martin et al. (2009) ( $0.94' \pm 0.2'$ ). With our new distance estimate (853 kpc), we constrain the physical size of And XXII to be  $255 \pm 78$  pc.

## 3.2 Spectroscopy

### 3.2.1 Membership

A CMD of stars derived from the CFHT-MegaCam imaging within a two arcminute radius of And XXII is shown in Figure 2. Spectroscopically targeted stars and likely member stars are highlighted. The red giant branch is clearly visible, while in the  $g$ -band data, even the horizontal branch is well detected (Figure 3). The velocity distribution of stars in And XXII is shown in Figure 5, highlighting the clear peak of 10 stars near  $-130 \text{ km s}^{-1}$ , representing And XXII (spectra are shown in Figure 6). The stars are also shown as a function of radius from the centre of the dwarf, with multiples of the half-light radius indicated. The probability that a given star is a member of And XXII is determined from a combination of its radial velocity, its distance from the RGB locus in the CMD, and its radial distance from the centre of And XXII. The motivation and methodology of the membership probability assignment is described in detail in Collins et al. (2012). These probabilities are listed in Table 2 for member stars, and reveal that the two outlying candidate stars at four half-light radii have a very low chance of

being members of the dSph, but the others are likely to be members.

### 3.2.2 Radial velocity and dispersion

The maximum likelihood approach provides a method to assess the true underlying velocity distribution of the dSphs even when the velocity errors for member stars are large and variable (see, for example, Martin et al. 2007), which is the case here. In our analysis, we weight each member star by its probability (Table 2), as described in detail in Collins et al. (2012). Figure 7 shows the likelihood distribution as a function of the mean motion  $v_r$  and velocity dispersion  $\sigma_v$  of And XXII. The dispersion is not quite resolved at the  $1\sigma$  level. We find  $v_r = -130.0 \pm 1.7 \text{ km s}^{-1}$  and  $\sigma_v < 6.0 \text{ km s}^{-1}$  at 99.5% confidence, formally consistent with zero. This in line with other M31 dSphs (see, for example, Tollerud et al. 2012, Collins et al. 2010, 2012). Specifically, Tollerud et al. (2012) find  $v_r = -126.8 \pm 3.1 \text{ km s}^{-1}$  and  $\sigma_v = 3.54^{+4.16}_{-2.49} \text{ km s}^{-1}$  from a sample of seven stars, in agreement with our findings.

Photometric metallicity,  $[\text{Fe}/\text{H}]_{\text{phot}}$ , is estimated by comparison to Dartmouth isochrones (Dotter et al. 2008) corrected for extinction and shifted to the distance of And XXII. This  $[\text{Fe}/\text{H}]$  value is shown in Figure 5 as a function of radial velocity, revealing the tight range in metallicities for most stars in And XXII (median  $[\text{Fe}/\text{H}] = -1.6$ , interquartile range  $\pm 0.1$ ).

One-dimensional spectra of the most robust member stars in And XXII are shown in Figure 6. All spectra show CaT cross-correlation peak  $> 0.2$ , and lie on the well defined RGB of And XXII. The inverse variance weighted, summed spectrum is shown in the bottom offset panel. While not shown in the spectra, the NaI doublet is significantly undetected in the individual stars, and also in the stacked spectrum. The NaI equivalent width is sensitive to the surface gravity, and thus is a good discriminant of Galactic foreground dwarf stars (Schiavon et al. 1997). Stars with velocities  $> -100 \text{ km s}^{-1}$ , typical Galactic star velocities, often have well detected NaI doublet lines in our DEIMOS spectra. At the velocity of And XXII,  $\sim -130 \text{ km s}^{-1}$ , the typical fraction of Galactic stars has already dropped close to zero (e.g., Collins et al. 2012), and only one star in our CMD selection box, lying within two core radii of And XXII, is obviously Galactic with strong NaI equivalent width. The spectroscopic  $[\text{Fe}/\text{H}]$  has very large errors in most of the individual spectra, however a reasonable comparison can be made between the  $[\text{Fe}/\text{H}]$  derived from the stacked spectrum and the median photometric  $[\text{Fe}/\text{H}]$ . We find  $[\text{Fe}/\text{H}] = -1.62$  by measuring the EW of the CaII triplet lines as in Chapman et al. (2005), on the Carretta & Gratton (1997) scale. Koch et al. (2008) have also demonstrated that high quality Keck/DEIMOS spectra of stars in the M31 halo are amenable to further chemical analysis, showing a range of species (mostly FeI and TiI lines) which become weaker for the more metal-poor stars. Our stacked spectra do not detect significant absorption at the TiI lines (8378, 8426, and 8435 Å), but consistent with the expected equivalent widths for stars of similar metallicity from Koch et al. (2008).

#### 4 RESULTS – EC1 AND EC2

We next turn our attention to the two extended clusters EC1 and EC2, which were recently discovered in the halo of M33. As discussed in the introduction, extended clusters (Huxor et al. 2005, 2008, 2009) could have several viable explanations: compact, tidally perturbed dwarf galaxies, clusters associated to stellar debris from low surface brightness dSphs that have been disrupted, or simply large clusters.

The M33 extended clusters, EC1 (Stonkute et al. 2008) and EC2 (Huxor et al. 2009), are neither as luminous, nor as extended as the extended cluster EC4 in the halo of M31, studied in detail by Collins et al. (2009). We obtained spectra for only a few RGB stars in M33-EC1 and EC2 since most of the stars in these systems were either too faint or too crowded in the field to permit multiple slits being placed. In Figure 8, we show the stars in the 5 arcmin<sup>2</sup> field around each cluster, although blending in the central cluster regions results in not all cluster stars being extracted by our cataloging – the reader is referred to the EC1 HST data in Stonkute et al. (2008). The figure shows the small core radii for the two ECs (20.3 and 18.0 pc respectively) and the dearth of stars suitable for spectroscopic followup. While a spectroscopic slit is placed over the brightest star in each EC, along with fainter neighbouring stars on the slit, the next spectroscopically accessible bright star is beyond the core radius in each case. With a single spectroscopic mask, it is therefore difficult to study these faint, relatively compact systems.

In Figure 9, we show the distribution of velocities of observed stars in the EC1 and EC2 fields. As expected from Figure 8, the vast majority of targeted stars lie at large radial distances and are almost certainly unrelated to the ECs. We can in fact only differentiate the EC stars from the field by plotting the velocities against their radius from the EC centres (middle panels of Figure 9). Here, our central targeted star in each EC is apparent, with velocities of  $-152.0 \pm 4.5$  km s<sup>-1</sup> (EC1) and  $-200.2 \pm 5.8$  km s<sup>-1</sup> (EC2). In the case of EC1, a star lying 15'' away ( $\sim 60$ pc – 3 core radii) is identified as a second candidate member, by velocity ( $-149.3 \pm 7.2$  km s<sup>-1</sup>) and colour lying on the identified RGB of Stonkute et al. (2008). However, adopting the membership probability criteria of Collins et al. (2012), this star is unlikely to be a member. Given the possible tidal-disrupted nature of the ECs however, this star may be a former member of the cluster, one that is no longer bound. In the EC2 field, no other members are identified. Finally, the spectroscopically derived [Fe/H] from the CaT lines is shown as a function of radial velocity in Figure 9, revealing comparable metal-poor [Fe/H]’s ( $\sim -1.5$  in all cases) to that published for the two ECs.

In Figure 10, we show the individual spectra of the plausible EC1 and EC2 members, revealing well detected CaT lines and reliable systemic velocity measurements. Clearly no dispersion estimates are possible here. It is conceivable that the bright identified star in the spectrum is actually a composite of several cluster stars. If so, the line width would provide an indication of the stellar velocity dispersion. However with  $\sim 40$  km s<sup>-1</sup> resolution, and with the spectra clearly dominated by the brightest targeted star, we cannot hope to resolve any significant line width (nor do we).

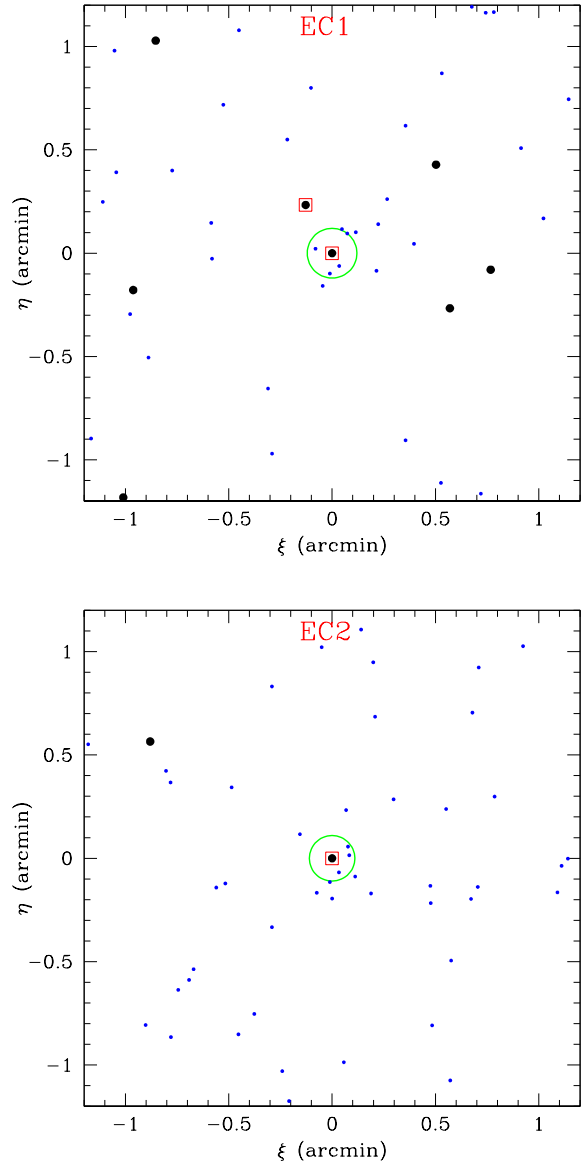


**Figure 8.** Spatial distribution of stars in the regions around EC1 (top) and EC2 (bottom). Stars with colours and magnitudes consistent with metal-poor red giant branch populations at the distance of M33 (blue dots) reveal the small concentrations associated to EC1 and EC2. Blending in the central cluster regions results in not all cluster stars being extracted by our cataloging (as depicted above). All stars lying in the DEIMOS mask are shown (large black circles), while candidate member stars identified spectroscopically are highlighted (red squares). The central circle highlights the core radii in each case.

The only other extended cluster in the M31 system that has been studied to date spectroscopically is EC4 (Collins et al. 2009), which clearly resides in the M31 halo. These authors presented a spectroscopic survey of candidate RGB stars in the extended star cluster, EC4, overlapping two M31 tidal streams. Six stars lying on the red giant branch within 2 core-radii of the centre of EC4 were found to have an average  $v_r = -287.9^{+1.9}_{-2.4}$  km s<sup>-1</sup> and  $\sigma_{v,corr} = 2.7^{+4.2}_{-2.7}$  km s<sup>-1</sup>, with a resulting mass-to-light ratio

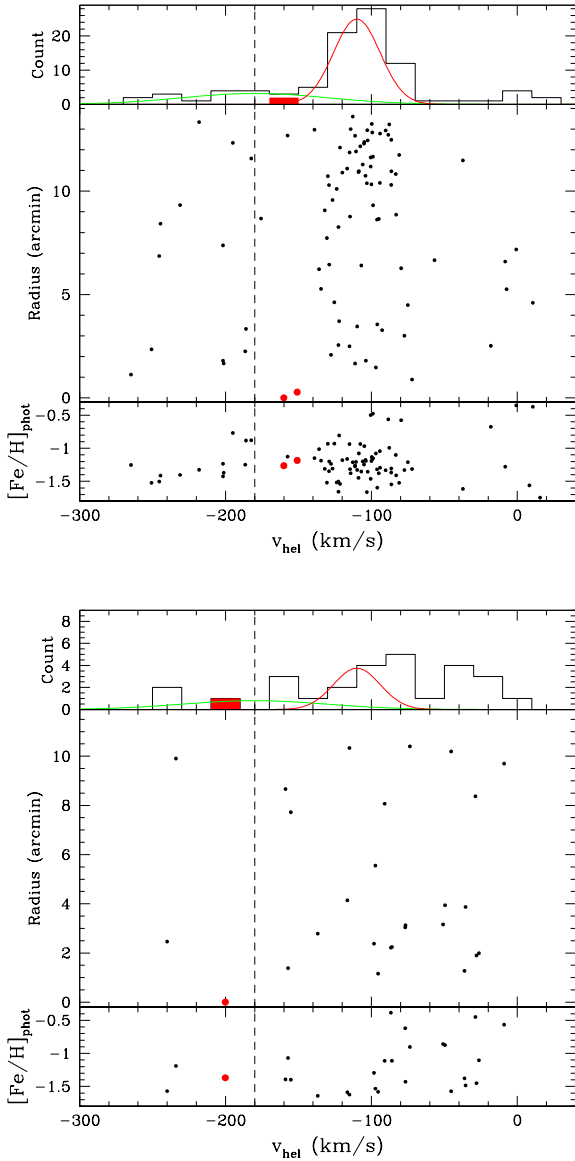


**Figure 9.** The distribution of stars in the fields of EC1 (top) and EC2 (bottom) as a function of their radial velocity, where two likely member stars are found for EC1, and only one member star for EC2, shaded red (upper panels). The M33 systemic velocity ( $-179 \text{ km s}^{-1}$ ) is shown (dashed line). For EC1, the best fit halo (green) and disk (red) populations are shown as Gaussian curves,  $\sigma_{V,halo} = 52 \text{ km s}^{-1}$  at systemic velocity, and  $\sigma_{V,disk} = 16 \text{ km s}^{-1}$  at  $-110.3 \text{ km s}^{-1}$ , after removing likely Milky Way stars (see Trethewey 2011 for details). For EC2, we show the same Gaussian curves scaled to the stars which are not likely to be Milky Way by velocity and location in the CMD. In the middle panels, the stars are then shown as a function of radius from the centres of the ECs, where half-light radius is only  $\sim 20 \text{ pc}$  ( $\sim 5''$ ) in each case. Photometric  $[\text{Fe}/\text{H}]$  as described in the text is shown on the bottom panels, revealing the ECs to have likely  $[\text{Fe}/\text{H}] \sim -1.3, -1.5$  respectively, consistent with their RGBs from the CMDs in Huxor et al. (2009, 2010).

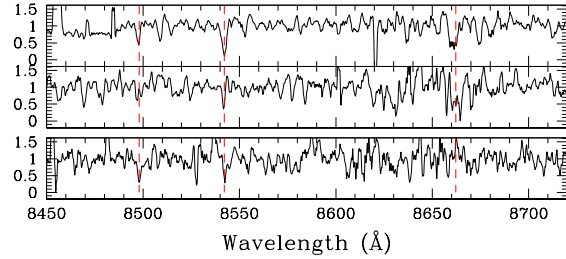


**Figure 10.** The individual spectra of the two EC1 members (above), and the EC2 member (below), are displayed. All three spectra have robust cross correlations with the CaT lines, but as can be seen, the third CaT line is noisy as a result of poor sky subtraction.

for EC4 of  $M/L = 6.7^{+15}_{-6.7} M_{\odot} / L_{\odot}$ , a value that is consistent with a globular cluster within the  $1\sigma$  errors. Considering several formation and evolution scenarios which could account for our kinematic and metallicity constraints on EC4, they conclude that EC4 is most comparable with an extended globular cluster rather than a dark matter dominated galaxy. However they find that both the kinematics and metallicity of EC4 bear a striking resemblance to M31’s tidal stream ‘Cp’ (Ibata et al. 2007; Chapman et al. 2008), as described in the introduction, motivating a search for similar tidal structures around EC1 and EC2.

We have searched the regions around EC1 and EC2 for relative overdensities of stars compared to the disk and halo projected profiles (Cockcroft et al. 2012), however we find no conclusive evidence for either lying in a clear overdensity. EC1 is close enough to the outer disk and stellar tidal tails of M33 that it is difficult to make an assessment. The  $0.5 \text{ deg}^2$  field surrounding EC2 is within  $1\sigma$  the density of the halo profile estimate of Cockcroft et al. (2012).

In velocity space, we also do not find any obvious evidence for sharp, kinematic stream-like structure (cold velocity spikes) around either EC1 or EC2 (as was found for M31-EC4), except for the second star at 3 core radii in EC1 discussed above. Figure 9 also shows that neither of the ECs is rotating with the disk population, which is  $V_{\text{helio}} \sim -110 \text{ km s}^{-1}$  at the location of EC1 (uncorrected for disk inclination), with  $\sigma_{V,disk} = 16 \text{ km s}^{-1}$  after removing likely Milky Way stars, comparable to that found in McConnachie et al. (2006) and Trethewey (2011), suggesting that they are true satellites within the M33 halo. For EC1, the best fit halo and disk populations are shown as Gaussian curves,  $\sigma_{V,halo} = 52 \text{ km s}^{-1}$  at systemic velocity, and  $\sigma_{V,disk} = 16 \text{ km s}^{-1}$  at  $-110.3 \text{ km s}^{-1}$ , after removing likely Milky Way stars (see Trethewey 2011 for details). In EC2 it is not clear that the disk is still kinematically identified from the MW foreground (Trethewey 2011), and we show the same Gaussian curve scaled to the stars not likely to be foreground (identified by velocity and location in the CMD).

However, EC1 does seem to reside within a cloud of apparent ‘halo’ stars in M33. A kinematic ‘halo’ component was first discovered in M33 from the spectroscopic survey in McConnachie et al. (2006). In the EC1 field, this halo component is well detected and peaks near the M33 systemic



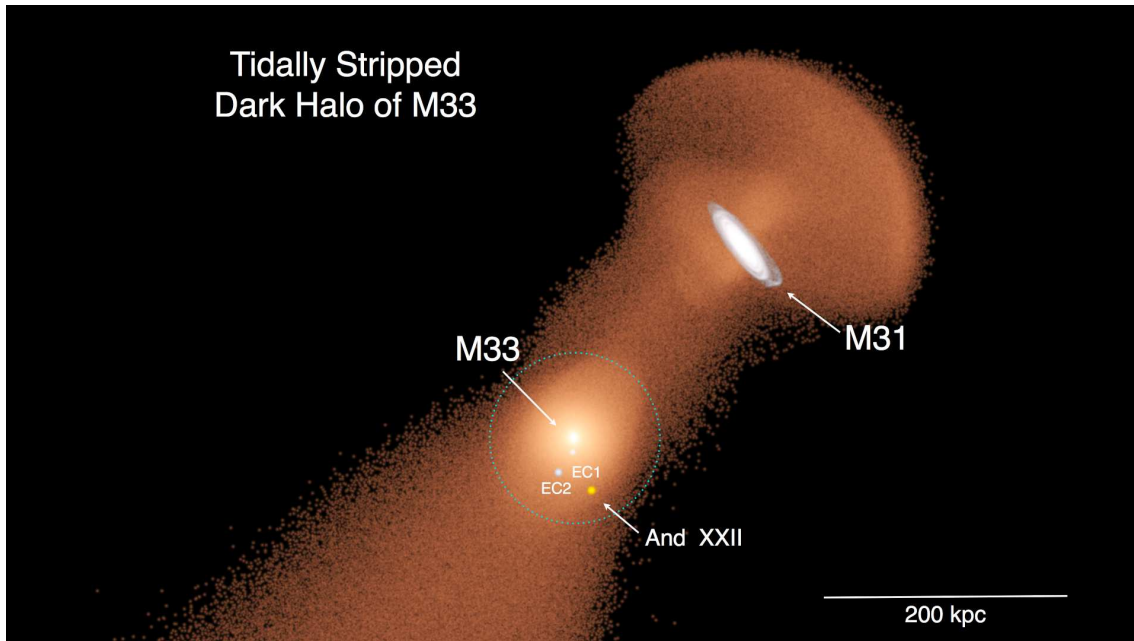


**Figure 11.** A model of the distribution of dark matter for M33 after an interaction with M31. The initial dark matter halo of M33 was tidally truncated at a radius of 70 kpc with a total mass of  $1.1 \times 10^{11} M_{\odot}$ . The disk and bulge of the M31 n-body model is shown for reference though the dark halo of M31 is intentionally not shown to reveal the expected distribution of M33 halo mass after the interaction. We also draw a circle of radius 70 kpc around M33 representing the tidal radius in this model. After the encounter, approximately 40% of the initial dark halo mass of M33 is stripped off and either falls back onto M31 or is flung towards the SW direction. The current positions of And XXII, EC1 and EC2 are shown in their observed relative positions to M33 in the model. And XXII lies near the edge of the tidal radius in projection in this post-interaction model of the halo of M33 while EC1 and EC2 still appear to be in the halo. An animation of the rotation of the model shows that each of And XXII, EC1 and EC2 are near the tidal radius of the stripped M33 halo (<http://www.ast.cam.ac.uk/~schapman/and22.mov>). If this scenario is correct, these objects were probably more tightly bound to M33 prior to the interaction and are either just barely bound now or are just about to escape from M33 due to tidal stripping.

velocity of  $-179$  km/s, with a best fit  $\sigma_{V,halo} = 52$  km s $^{-1}$ . Trethewey (2011) have demonstrated that the ‘halo stars’ in the EC1 field represent a clear overdensity relative to the radial profile of this halo component (derived from the stars centred about the systemic velocity in 14 other spectroscopic fields along the major axis of M33). However, this relatively strong M33 ‘halo’ component ( $\sim 5\%$  of the disk density) may more likely be a distorted or disrupted disk component as result of the encounter with M31, or even a very high dispersion thick disk component identified as in M31 (Collins et al. 2011b). This hypothesis is strengthened by the recently discovered stellar halo in M33 identified photometrically (Cockcroft et al. 2012), which appears substantially weaker ( $\sim 1\%$  of the disk density) than the spectroscopically identified ‘halo’ population centred about the systemic velocity.

## 5 DISCUSSION

In this section we address the question of whether And XXII is a satellite of M33. As we will see, our distance and radial velocity determinations play a key role in the discussion. We also consider constraints on the mass of M33 from the known satellites in its outer halo.

### 5.1 Simulation of the M31-M33 interaction

As part of the PAndAS project, we have run a series of simulations to explore the hypothesis that M33 passed within  $\leq 60$  kpc of M31 at some stage during the past few Gyrs. This hypothesis was proposed to explain the existence of stellar debris in the outskirts of the M33 disk (McConnachie et al. 2009, Dubinski et al., in preparation).

The initial conditions for M31 and M33 are generated using the GalactICS code (Kuijken & Dubinski 1995, Widrow, Pym, & Dubinski 2008) and comprise three collisionless components: an exponential disk, a Sersic bulge, and an extended dark matter halo. The models generated by this code are specified in terms of the phase space distribution functions (DFs) for the different components. The DFs in turn are built out of functions of the integrals of motion and therefore, through Jeans theorem, provide equilibrium solutions. In the current version of the model, it is assumed that the velocity distribution of the halo particles is isotropic and that their DF depends only on the energy.

The density profile for the halo is given by

$$\rho(r) = \frac{\rho_0}{r/a (1 + r/a)^\beta} T(r_{\text{out}}, \delta r_{\text{out}}) \quad (2)$$

where  $a$  and  $\rho_0$  are, respectively, the scale length and density parameter for the halo while  $\beta$  controls the power-law fall-off of the density at large radii. The function  $T$  varies smoothly from 1 to 0 and has the effect of truncating the halo at a radius  $\sim r_{\text{out}}$  over a range in radii of a few  $\delta r_{\text{out}}$ . The

distribution function for the halo is determined from the density profile via as Abel transform.

The structural parameters of the different components are adjusted so that the composite models match the surface brightness profiles and rotation curves for the two galaxies. For M31, we use the composite rotation curve from Widrow:2003 and the surface brightness profile from Waltherbos:1987 while for M33, we use the rotation curve from Corbelli:2003 and the surface brightness profile from Regan:1994. We follow cosmological arguments from Loeb et al. (2005) and tune the M31 model parameters so that the halo mass within 280 kpc is  $M = 2.5 \times 10^{12} M_{\odot}$ . The key structural parameters for the two galaxies are given in Table 1 of McConnachie:2009.

Candidate orbits for M33 are found by first modelling M33 as a test particle that moves under the influence of the M31 gravitational field and dynamical friction. The latter is incorporated in the calculation via the Chandrasekhar formula where the Coulomb logarithm is calibrated using N-body simulations. We search the space of orbits to find initial conditions that lead to a strong encounter between M33 and M31 and also to a present-day position and velocity of M33 that are consistent with observational constraints. Representative candidate orbits are then simulated using standard N-body methods. The simulations are fully self-consistent in the sense that all components of both M31 and M33 are “live” (i.e., the potentials evolve). Both M33 and M31 halos were simulated with 2M particles.

For M33, the tidal radius at the initial position of a typical candidate orbit is  $\approx 70$  kpc and so we set parameters of the function  $T$  so that the halo is truncated at that radius. We also ran a 50 kpc truncation radius model and the results are similar. Our M33 model has a halo mass of  $1.1 \times 10^{11}$  solar masses. The modeling details are laid out in Dubinski et al. (in prep).

In this paper, we focus on a particular example in which M33 passes within 50 kpc of the M31 centre. The distribution of dark matter for M33 after an interaction with M31 is shown in Fig. 11. The disk and bulge of the M31 n-body model is shown for reference though the dark halo of M31 is intentionally not shown to reveal the expected distribution of M33 halo mass after the interaction. After the encounter approximately, 40% of the initial dark halo mass of M33 is stripped off and either falls back onto M31 or is flung towards the SW direction.

## 5.2 Is And XXII a Satellite of M33?

The assumption that satellites trace dark matter deserves careful scrutiny. In the hierarchical clustering scenario, the dark matter halos associated with galaxies such as M31 grow by accreting smaller subhalos. Though most of the subhalos are tidally disrupted, some survive and a fraction of these will harbour the satellite galaxies observed today. Thus, the spatial distribution of satellite galaxies vis-a-vis the dark matter depends on the distribution of surviving subhalos and the distribution of satellites in comparison with the subhalos.

Numerical simulations of structure formation in a pure dark matter universe suggest that subhalos are less concentrated than the dark matter (Ghigna et al. 2000, Gao et al. 2004, Diemand et al. 2004, DeLucia et al. 2004), presum-

ably because the subhalos in the inner regions of the parent halo are more susceptible to tidal disruption. On the other hand, satellites are more robust than their pure dark matter counterparts (Nagai et al. 2005, Libeskind et al. 2010). These results may explain why Sales et al. 2007 find that the spatial distribution and kinematics of the satellites and dark matter in their cosmological simulations are very similar.

In addressing the question of whether And XXII is a satellite of M33, we make the assumption that satellites trace dark matter. Therefore, the ratio of the phase space density of M33 halo particles at a given position and velocity to that of M31 provides an estimate of the probability that a satellite with these phase space coordinates is a satellite of M33 relative to the probability that it is a satellite solely of M31. (Since M33 is very likely a satellite of M31, any satellite of M33 is also a member of the M31 system.) Of course, in calculating this probability, we must marginalize over unknown quantities such as the proper motion of And XXII.

In Fig. 11, the current positions of And XXII, EC1 and EC2 are shown in their observed relative positions to M33 in the model. And XXII can be seen to lie near the edge of tidal radius in projection in this post-interaction model of the halo of M33 while EC1 and EC2 still appear to be in the halo. An animation of the rotation of the model shows that each of And XXII, EC1 and EC2 are near the tidal radius of the stripped M33 halo. If this scenario is correct, these objects were probably more tightly bound to M33 prior to the interaction and are either just barely bound now or are just about to escape from M33 due to tidal stripping. If M33 didn’t have the strong interaction implied by this simulation, then its halo would be more extended making And XXII even more likely to be a satellite.

Figure 12 shows a reduced phase space density of particles close to the And XXII line-of-sight that are initially part of either the M33 halo or M31 halo. The reduced phase space density corresponds to the number of stars per unit line-of-sight distance and unit radial velocity. We first select stars from either the M31 or M33 halo that lie within 0.01 rad of the line-of-sight to And XXII. These stars are then binned in terms of  $d_r$  and  $v_r$ . The number of stars in each bin divided by the phase space volume of the bin gives the desired density. We incorporate uncertainties in the distances to M31 and M33 using a simple Monte Carlo scheme whereby the above procedure is repeated for different choices of these distances, as prescribed by the quoted uncertainties.

We see that at the measured coordinates of And XXII, the M31 halo density is almost 1 dex lower than the M33 halo density. The implication is that And XXII is very likely associated with M33. While the uncertainty in distance to And XXII has a larger effect on the inferred density in M33 than in M31, the change to the probability is not large. Within the  $1\sigma$  distance uncertainties the M33/M31 density contrast never drops significantly below 1 dex. Nevertheless, improvements in the distance determination to And XXII will have the largest effect on resolving the question of whether it is a satellite of M33. A similar analysis of the extended clusters, EC1 and EC2, show the phase space densities of the M31 and M33 halos in the vicinities of these objects are comparable to And XXII within factors of a few (although the large radial distance of EC1 makes it the least

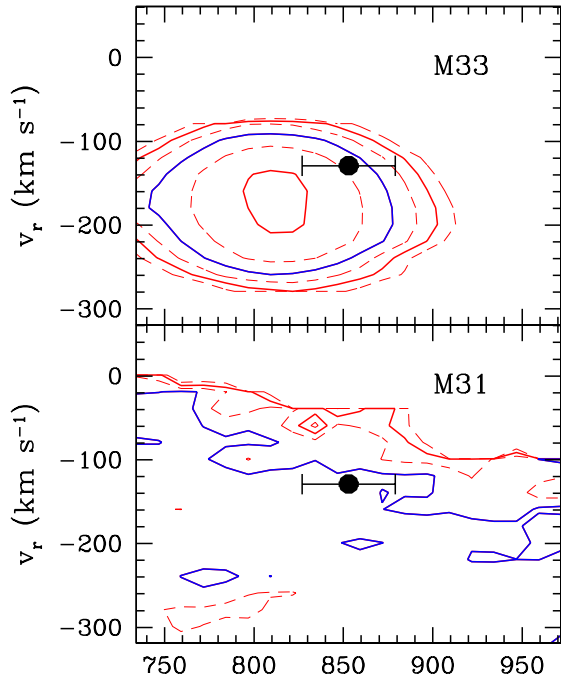


**Figure 12.** Phase space density,  $v_r$  ( $\text{km s}^{-1}$ ) versus  $d_r$  (kpc), of halo particles in M33 (top panel) and M31 (bottom panel). The upper panel gives the density for particles that are initially part of the M33 halo and remain so through the interaction with M31. Solid contours are spaced by 1 dex (dashed are at 0.5 dex). Levels are the same in both panels, with the blue line (drawn to go through And XXII in the M33 halo density) providing a reference between the two. A comparison of the two at the phase space position of And XXII (black filled circle with error bars on radial velocity and HB-distance) gives the probability for And XXII to be a satellite of M33 (and thus also a satellite of M31), as compared with the probability of it being only an M31 satellite, not associated with M33. We account for the uncertainty in the M31 and M33 distances (both 19 kpc – Conn et al. 2012), which spreads out the density distribution in distance  $d_r$ , especially for M33. The M31 halo has almost 1 dex lower density than M33 at this point, although the uncertainty in distance to And XXII has a larger effect on the relative density in M33 than M31.

likely of the three to be a satellite), thus all three objects are good candidates to be associated with M33.

In Figure 13, we plot the particles close to the And XXII line-of-sight (LOS) as a function of their kinetic energy  $K$  and binding energy  $P$ , where these quantities are calculated in the rest frame of M33. The diagonal line in the figure divides bound and unbound particles and reveals firstly that in the direction of And XXII, all of the particles initially in the M33 halo remain bound to M33, and secondly that some of the M31 particles become bound to M33. Further analysis is required to determine the extent to which M33 can sweep up M31 halo particles.

In McConnachie et al. (2009) we provided an animation of an M31-M33 encounter that included an extended stellar halo for M33. This animation showed that a signifi-

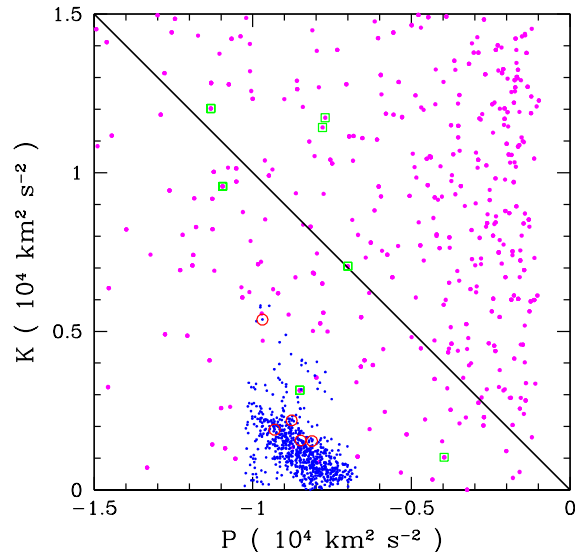


**Figure 13.** In this plot, we take the particles along the And XXII line of sight (LOS) and calculate their kinetic and potential energy with respect to M33. That is,  $K = 0.5s^2$  where  $s$  is the speed of a particle in the M33 frame of rest and  $P = -\text{potential energy}$  with respect to M33 particles. Magenta (blue) points are M31 (M33) halo particles in a cone along the LOS to And XXII, Green squares (Red circles) are the M31 (M33) particles within  $2\sigma$  error bars of our And XXII HB distance and velocity values, while the solid line divides bound and unbound particles.

cant number of halo particles were stripped from M33. The point here is that the particle distribution in the cone along the And XXII line-of-sight is dominated by material that is still bound to M33 and that only a few particles are caught in the act of being tidally stripped. Most of the stripped particles seen in the simulation are at projected distances from M33 much larger than the projected radius of And XXII.

### 5.3 Constraining the mass of M33 with its satellites

In Figure 14 we compare the projected radius and radial velocity for And XXII, EC1 and EC2 with the escape velocity,  $v_{\text{esc}} \equiv \pm\sqrt{2|\phi|}$  as derived from our M33 model, where  $\phi$  is the spherical approximation to the gravitational potential. Also shown are curves  $v_{\text{esc}}/\sqrt{3}$  where the factor of  $1/\sqrt{3}$  is included to account for the fact that the radial velocity is one of three components. Figure 14 contrasts the initial conditions with the present-day distribution, where the escape speed decreases with time due to tidal stripping of M33 during its encounter with M31. The projected distance represents a lower bound on the true physical distance of an object to the M33 centre. In fact, the animation in Figure 11 reveals that each of And XXII, EC1 and EC2 is near the tidal radius of the stripped M33 halo at their true distances, with EC1 being the most distant satellite of the three at 71.2 kpc. All three objects have radial velocities relative to M33 that are below the apparent escape speed, emphasizing further that they are very likely bound satellites, although And XXII comes close to the  $v_{\text{esc}}/\sqrt{3}$ . These

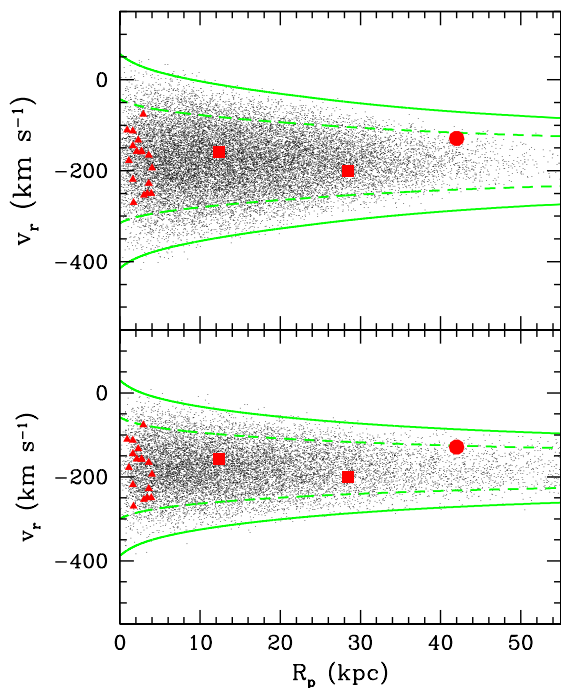


**Figure 14.** Distribution of M33 objects in terms of the projected radius and radial velocity. AndXXII is shown as the large blue circle while EC1 and EC2 are shown as the blue squares. Blue triangles show the positions of all *halo* globular clusters (GCs) from Chandar et al. (2002) (i.e., GCs with  $|V_{\text{disk}} - V_{\text{GC}}| > 70 \text{ km s}^{-1}$ ). Black dots are from the simulations where the top panel is for initial conditions and the bottom panel is for the present-day distribution. The solid red curves give an estimate of the escape speed from M33 shifted to the Galactic frame,  $v_{\text{esc}} - 179 \text{ km s}^{-1}$  where  $v_{\text{esc}} \equiv \sqrt{2\phi}$  and  $\phi$  is the spherical approximation to the gravitational potential. The dashed red curves use  $v_{\text{esc}}/\sqrt{3}$  to roughly account for the fact that the radial velocity is one of three velocity components. Note that the escape speed decreases with time due to tidal stripping of M33 during its encounter with M31.

results suggest that the fiducial dynamical mass estimates for M33 ( $\sim 10^{11} M_{\odot}$ ) are consistent with the M33 outer satellite system. By contrast, M31 appears to have several satellites that have radial velocities at or above the nominal escape velocity (Chapman et al. 2007).

Cockcroft et al. (2011) extended previous studies of Globular Clusters (GCs) in M33 (Huxor et al. 2009) out to a projected radius of 50 kpc and covers over 40 square degrees. They found only one new unambiguous star cluster (at a projected radius of 22 kpc) in addition to the five previously known in the M33 outer halo (ranging from 9 kpc to 28 kpc). In total then, other than these three objects, there are only 3 other satellites (all GCs) in the 10-50 kpc halo of M33. To fill in the inner region of the plot, we also show the ‘halo’ GCs from Chandar et al. (2002) defined to have  $|V_{\text{disk}} - V_{\text{GC}}| > 70 \text{ km s}^{-1}$ .

Figure 14 also provides a visual depiction of the evolution of M33 halo particles and the relation between AndXXII and the halo particles. The effect of the encounter is to populate regions with low binding energy, as expected.

The simulation also shows that the curves illustrating the escape velocity of the M33 potential are a reasonable approximation to the projected 3D properties of the bound satellite GCs and dSph. In the panel depicting the system after the encounter, there is a much higher density of halo particles bound to M33 at the position of AndXXII. While AndXXII may well be a satellite of M33, its phase space position was likely affected by M31 during the M33-M31 encounter.

## 6 CONCLUSIONS

We have explored the association between M33 and three possible satellites, AndXXII, EC1, and EC2, finding all three were likely to have originally been bound to M33, and likely still are, depending on the nature of the interaction of M31-M33. From a spectroscopic survey of these candidate satellites, we have defined probable members, for which we derive radial velocities down to  $i \sim 23$ , and with average errors of  $5 \text{ km s}^{-1}$ . The AndXXII heliocentric velocity is  $v_r = -130.0 \pm 1.7 \text{ km s}^{-1}$ ,  $+177 \text{ km/s}$  relative to M31, but only  $+50 \text{ km/s}$  relative to M33 (in agreement with Tollerud et al. 2012,  $v_r = -126.8 \pm 3.1 \text{ km s}^{-1}$ ). The dispersion is unresolved with 10 member stars at  $\sigma_v < 6.0 \text{ km s}^{-1}$ , 99.5% confidence. Using the photometry and spectroscopy of the confirmed member stars, we find a metallicity with median  $[\text{Fe}/\text{H}] = -1.6 \pm 0.1$ . Our identified member stars in AndXXII along with an assessment of the horizontal branch peak suggest a radial distance of  $853 \pm 26 \text{ kpc}$ .

For the two extended clusters in M33, we also find systemic velocities of  $-152.0 \pm 4.5 \text{ km s}^{-1}$  (EC1) and  $-200.2 \pm 5.8 \text{ km s}^{-1}$  (EC2). EC1 is further found to lie in a local kinematic overdensity of apparent halo stars in M33, suggesting it may be a signpost for a recently disrupted dSph satellite of M33.

The combined velocity and distance information is used to assess whether AndXXII, EC1, and EC2 could have been, or are still bound satellites of M33 using our simulations of the M31-M33 interaction. We conclude that all three are highly likely to have originally been satellites of M33. All three satellites have radial velocities relative to M33 below the apparent escape speed, and modelling of a possible M33-M31 interaction indicates that all three satellites lie near the model virial radius,  $\sim 70 \text{ kpc}$ , suggesting they could be close to the point of being bound to M33 if tangential velocities were comparable to radial velocities. If M33 didn’t have the strong interaction implied by our simulation, then its halo would be more extended making the AndXXII, EC1, and EC2 even more likely to be satellites. The fiducial dynamical mass estimates for M33 ( $\sim 10^{11} M_{\odot}$ ) are consistent with the M33 outer satellite system.

## ACKNOWLEDGMENTS

SCC thanks the STFC for financial support. RAI gratefully acknowledges support from the Agence Nationale de la Recherche through the grant POMME (ANR 09-BLAN-0228). GFL thanks the Australian Research Council for support through his Future Fellowship (FT100100268) and

Discovery Project (DP110100678). JP acknowledges support from the Ramón y Cajal Program as well as by the Spanish grant AYA2010-17631 awarded by the Ministerio de Economía y Competitividad. The data presented herein were obtained at the W.M. Keck Observatory, which is operated as a scientific partnership among the California Institute of Technology, the University of California and the National Aeronautics and Space Administration. The Observatory was made possible by the generous financial support of the W.M. Keck Foundation. Based on observations obtained with MegaPrime/MegaCam, a joint project of CFHT and CEA/DAPNIA, at the Canada-France-Hawaii Telescope (CFHT) which is operated by the National Research Council (NRC) of Canada, the Institut National des Sciences de l'Univers of the Centre National de la Recherche Scientifique of France, and the University of Hawaii.

## REFERENCES

- Belokurov, V., Zucker, D. B., Evans, N. W., Wilkinson, M. I., Irwin, M. J., Hodgkin, S., Bramich, D. M., Irwin, J. M., et al., 2006, *ApJ*, 647, L111
- Belokurov V. et al., 2007, *ApJ*, 654, 897
- Carretta, E., Gratton, R. 1997, *A&AS* 121, 95
- Chandar, R., Bianchi, L., Ford, H.C., Sarajedini, A., 2002, *ApJ*, 564, 712
- Chapman S., Ibata R., Ferguson A. M. N., Lewis G., Irwin M. & Tanvir N. 2005, *ApJ* 632, L87
- Chapman S., Ibata R., Lewis G., Ferguson A. M. N., Irwin M., McConnachie A., Tanvir N. 2006, *ApJ* 653, 255
- Chapman S., Penarrubia J., Ibata R., McConnachie A., Martin N., Irwin M., et al., 2007, *ApJ* 662, 79L
- Chapman, S. C.; Ibata, R.; Irwin, M.; Koch, A.; Letarte, B., et al., 2008, *MNRAS*, 390, 1437
- Cockcroft, R., et al., 2011, *AJ*, 730, 112
- Cockcroft, R., et al., 2012, *AJ*, submitted
- Collins, M., et al., 2012, submitted
- Collins, M., et al., 2011a, *MNRAS*, 417, 1170
- Collins, M., et al., 2011b, *MNRAS*, 413, 1548
- Collins, M., et al., 2010, *MNRAS*, 407, 2411
- Collins, M., et al., 2009, *MNRAS*, 396, 1619
- Conn, A., et al., 2012, *MNRAS*, in press
- Corbelli, E. 2003, *MNRAS*, 342, 199
- De Lucia, G., Kauffmann, G., Springel, V., et al. 2004, *MNRAS*, 348, 333
- Diemand, J., Moore, B., & Stadel, J. 2004, *MNRAS*, 352, 535
- Dotter, A., Chaboyer, B. Jevremovic, D., Kostov, V. Baron, E.; Ferguson, J.W. 2008 *ApJS*, 178, 89
- Erickson, Lance K.; Gottesman, S. T.; Hunter, James H., Jr. 1999 *ApJ*...515..153
- Evans, N. W. & Wilkinson, M. I. 2000, *MNRAS*, 316, 929
- Faber, S. M., et al., 2003, *SPIE*, 4841, 1657
- Gao, L., White, S. D. M., Jenkins, A., Stoehr, F., & Springel, V. 2004, *MNRAS*, 355, 819
- Ghigna, S., Moore, B., Governato, F., et al. 2000, *ApJ*, 544, 616
- Guo, Qi; White, Simon; Boylan-Kolchin, Michael; De Lucia, Gabriella; Kauffmann, Guinevere; Lemson, Gerard; Li, Cheng; Springel, Volker; Weinmann, Simone 2011 *MNRAS*.tmp..164G
- Huxor A. et al. 2005, *MNRAS*, 360, 1007
- Huxor A. et al. 2008, *MNRAS*, 385, 1989
- Huxor, A., et al., 2009, *ApJ* 698, L77
- Ibata R., Chapman S., Ferguson A., Lewis G., Irwin M., McConnachie A., Tanvir N., 2004, *ApJ*
- Ibata R., Chapman S., Ferguson A., Lewis G., Irwin M., McConnachie A., Tanvir N., 2005, *ApJ* 634, 287
- Ibata R., Chapman S., Irwin M., Lewis G. & Martin N., 2006, *MNRAS* 373, 70L
- Ibata, R.; Martin, N. F.; Irwin, M.; Chapman, S.; Ferguson, A. M. N.; Lewis, G. F.; McConnachie, A. W. 2007, *ApJ* 671, 1591
- Kuijken, K., Dubinski, J., 1995 *MNRAS*, 277, 1341
- Koch, A., et al., 2008, *ApJ*, 689, 958
- Libeskind, N. I., Yepes, G., Knebe, A., et al. 2010, *MNRAS*, 401, 1889
- Loeb, A., Reid, M.J., Brunthaler, A. Falcke, H., 2005 *ApJ*, 633, 894L
- Mackey, D., Huxor, A. P., Ferguson, A. M. N., Irwin, M. J., Tanvir, N. R., et al., 2010 *ApJ*, 717L, 11
- Martin N. F., Ibata R. A., Irwin M. J., Chapman S. C., Lewis G. F., Ferguson A. M. N., Tanvir N. & McConnachie A. W., 2006, *MNRAS* 371, 1983
- Martin N. F., Ibata R. A., Chapman S. C., Irwin M. J., Lewis G. F., 2007, *MNRAS* 380, 281
- McConnachie, A., Irwin, M., Ferguson, A., Ibata, R., Lewis, G., Tanvir, N., 2004, *MNRAS* 350, 243
- McConnachie, A., Chapman, S., Ibata, R., et al., 2006, *ApJ*, 647L, 25
- McConnachie, A., et al., 2009, *Nature*, 461, 66
- McConnachie, A., et al., 2010, *ApJ*, 723, 1038
- Nagai, D., & Kravtsov, A. V. 2005, *ApJ*, 618, 557
- d'Onghia E., et al., 2010, *ApJ*, 709, 1138
- Peñarrubia J., McConnachie A., Babul A., 2007, *ApJ*, 650, 33
- Peñarrubia J., McConnachie A., Navarro J., 2008a, *ApJ*, 672, 904
- Purcell, C., et al., 2009, *ApJ*, 694L, 98
- Putman, M., Peek, J. E. G., Muratov, A., Gnedin, O. Y., Hsu, W., et al., 2009, *ApJ*, 703, 1486
- Regan, M. W., & Vogel, S. N. 1994, *ApJ*, 434, 536
- Richardson, J., et al., 2011, *ApJ*, 732, 76
- Rogstad, D.H., Wright, M. C. H., Lockhart, I. A. 1976, *ApJ*, 204, 703
- Sales, L., et al., 2007a, *MNRAS*, 382, 1901
- Sales, L., et al., 2007b, *MNRAS*, 379, 1464
- Schiavon R. P., Barbuy B., Rossi S. C. F. & Milone A., 1997, *ApJ* 479, 902
- Stonkute, R., et al., 2008, 135, 1482
- Simon J., Geha M., 2007, *ApJ*, 670, 313
- Tiede, G., Sarajedini, A., Barker, M.K. 2004, *AJ*, 128, 224
- Tollerud, E., et al. 2012, *ApJ* 752, 45
- Trethewey, D., 2011, MSc Thesis, University of Cambridge
- Widrow, L., Pym, B., Dubinski, J., 2008, *ApJ*, 679, 1239
- Walterbos, R. A. M., & Kennicutt, R. C., Jr. 1987, *A&ASupp*, 69, 311
- Watkins, L., Evans, N.W., An, J.H., 2010, *MNRAS*, 406, 264
- Widrow, L. M., Perrett, K. M., & Suyu, S. H. 2003, *ApJ*, 588, 311

**Table 2.** Properties of candidate member stars in And XXII centered at  $\alpha = 01\text{h } 27\text{m } 39.6\text{s}$ ,  $\delta = 28^\circ 05' 29''$ .

$ID^a$	$\alpha$ (J2000)	$\delta$ (J2000)	$i - mag$	$g - i$	$D_{rad}^b$	$[F e/H]_{phot}^c$	$v_r$ ( $\text{km s}^{-1}$ )	probability <sup>d</sup>
57	01 27 41.10	28 05 34.4	21.65	1.23	1.11	-1.58	$-130.7 \pm 3.7$	0.958
76	01 27 37.34	28 05 54.4	23.24	1.12	0.76	-1.78	$-119.0 \pm 16.9$	0.774
42	01 27 40.26	28 05 20.2	22.88	1.05	0.10	-1.87	$-131.9 \pm 6.9$	0.737
24	01 27 43.63	28 04 52.0	23.34	1.07	0.97	-1.91	$-129.4 \pm 8.3$	0.698
60	01 27 35.48	28 05 37.2	22.15	1.24	1.02	-1.02	$-125.6 \pm 5.4$	0.666
29	01 27 47.09	28 04 58.5	23.02	1.04	1.63	-1.40	$-130.8 \pm 9.2$	0.366
77	01 27 37.77	28 05 54.4	21.66	1.39	0.69	-1.13	$-128.6 \pm 3.7$	0.282
95	01 27 34.17	28 06 30.9	22.29	1.26	1.69	-1.58	$-129.5 \pm 5.4$	0.251
53	01 27 35.21	28 05 29.9	20.87	0.65	1.15	—	$-113.2 \pm 1.9$	0.010
86	01 27 55.63	28 06 18.0	23.04	1.23	3.56	-1.68	$-133.9 \pm 9.3$	0.003
10	01 27 23.05	28 04 12.6	22.64	0.76	3.93	—	$-130.4 \pm 7.8$	0.001
6 <sup>e</sup>	01 27 42.66	28 04 1.6	20.42	0.63	1.55	—	$-155.2 \pm 7.8$	$<10^{-4}$
131 <sup>f</sup>	01 28 20.16	28 08 43.0	20.78	1.29	9.91	—	$-111.5 \pm 7.8$	$<10^{-4}$

<sup>a</sup> Stars are ordered by their membership probability (see below)

<sup>b</sup> Radial distance in arcmin from the centre of And XXII.

<sup>c</sup> Photometric  $[Fe/H]$  defined by fitting Dotter isochrones to the  $I, g$ -mags, as described in the text. ID#10 lies off the range of isochrones, but is at sufficiently large distance from And XXII that its probability of membership is miniscule, and it has no effect on the dispersion or systemic velocity estimates.

<sup>d</sup> Candidate member stars are assigned a probability of membership to And XXII, defined by a combination of velocity, distance from the RGB locus, and radial distance from the centre of And XXII (see Collins et al. 2012 for details).

<sup>e</sup> This star is not considered as a member star with its low probability based on both CMD position and velocity offset from systemic. It is likely an M33 halo star.

<sup>f</sup> This star is not considered as a member star with its low probability based mainly on its  $10'$  distance from the centre of And XXII.

**Table 3.** Properties of the candidate member stars in M33's EC1 and EC2, centered at (EC1)  $\alpha = 01\text{h } 32\text{m } 58.5\text{s}$ ,  $\delta = 29^\circ 52' 03''$ , (EC2)  $\alpha = 01\text{h } 35\text{m } 41.8\text{s}$ ,  $\delta = 28^\circ 49' 16''$ .

$ID$	$\alpha$ (J2000)	$\delta$ (J2000)	$i - mag$	$g - i$	$D_{rad}$	$[F e/H]_{spec}$	$v_r$ ( $\text{km s}^{-1}$ )
EC1:							
20	01 32 57.91	29 52 16.9	23.02	1.04	0.25	-1.48	$-149.3 \pm 7.2$
127	01 32 58.50	29 52 02.9	21.65	1.23	0.0	-1.59	$-152.0 \pm 4.5$
EC2:							
70	01:35:41.78	28:49:15.5	21.04	1.15	0.0	-1.54	$-200.2 \pm 5.8$